

Supporting Information for

Computational and Experimental Investigation of Alkene Hydrogenation by a Pincer-Type [P₂Si]Rh Complex: Alkane Release via Competitive σ -Bond Metathesis and Reductive Elimination

Matthew T. Whited,^{*,†} Michael J. Trenerry,^{†,§} Kaitlyn E. DeMeulenaere,^{†,§} and Buck L. H. Taylor,^{*,†,‡}

[†] Department of Chemistry, Carleton College, Northfield, Minnesota 55057, United States

[‡] Department of Chemistry, University of Portland, Portland, OR 97203, United States

Computational Methods	S2
Intrinsic Reaction Coordinates	S3
Figure S1. IRC analysis of TS18 (norbornyl isomerization from 17 to 19).....	S3
Additional Computed Structures	S5
Figure S3. Exo and endo hydrometallation transition states TS16 and TS16-endo	S5
Figure S4. Full reaction pathway of model catalyst 1 with H ₂ in the absence of alkene	S6
Figure S5. H ₂ -scrambling via σ -bond metathesis of norbornyl complex 21	S6
Figure S6. H ₂ -binding transition states leading to σ -complexes 13 and 21	S7
Tables of Computational Data	S8
Table S1. SCF Energies and thermal corrections for all structures	S8
Table S2. Energies of key structures using different standard-state concentrations.....	S9
Table S3. Energies of key structures with different methods	S10
Figure S7. ¹ H NMR spectrum of [C ^y P ₂ Si ^{Me}]Rh(H ₂) (C ^y 1-H₂).....	S11
Figure S8. ³¹ P NMR spectrum of [C ^y P ₂ Si ^{Me}]Rh(H ₂) (C ^y 1-H₂)	S12
Figure S9. ¹ H NMR spectrum of reaction product of [C ^y P ₂ Si ^{Me}]Rh(nbd) (C ^y 1-nbd) with HD	S13
Figure S10. ¹ H NMR spectra of headspace after reaction of C ^y 1-nbd under 1:1 H ₂ /D ₂ (1 atm) for 20 min in the presence (top) and absence (bottom) of excess (1000 equiv) norbornene	S14
Determination of Norbornane Isotopomer Distribution in HD Reactions	S15
Figure S11. Mass spectrum of norbornane.....	S15
Figure S12. Hydrogenation of norbornene under HD (1 atm, 25 °C)	S16
Figure S13. Hydrogenation of norbornene under HD (1 atm, 50 °C)	S17
Figure S14. Hydrogenation of norbornene under HD (0.25 atm, 50 °C)	S18

Computational Methods

The supplemental file structures.xyz contains the computed Cartesian coordinates of all of the molecules reported in this study. The file may be opened as a text file to read the coordinates, or opened directly by a molecular modeling program such as Mercury¹ for visualization and analysis.

DFT calculations were performed with Gaussian 09.² Computed structures are illustrated using CYLView.³

All structures in the manuscript were computed with the B97-D3BJ⁴ functional, using the def2-TZVP basis set and IEF-PCM model for diethyl ether. Density fitting was enabled using the W06 fitting set, which is designed for use with the def2-SVP and def2-TZVP basis sets.⁵ Initial trial calculations were performed at a lower level of theory: B97D/def2-SVP in the gas phase.

The nature of transition states was verified by the presence of a single imaginary frequency. In cases where the molecular motions were ambiguous along that imaginary frequency (e.g., **TS5** and **TS18**), IRC calculations were performed to verify the transition state connected to the appropriate intermediates.

Thermal corrections were calculated from unscaled vibrational frequencies at the same level of theory using a standard state of room temperature (298 K) and an elevated pressure (235 atm) to account for entropy effects in solution, as in Leitner's benchmark study.⁶

Gibbs free energies in Gaussian were calculated at the default pressure of 1 atm and corrected to higher pressures for solution-phase. The correction was made by adding $RT \ln(c_{\text{soln}}/c_{\text{gas}})$, or about 3.23 kcal/mol to the free energy of all structures, where c_{gas} is the standard molar concentration in the gas phase (0.0409 mol/L or 1 atm) and c_{soln} is the molar concentration of pure diethyl ether at room temperature (9.625 mol/L or 235 atm).

This treatment has been proposed to correct for the overestimation of the entropic cost of bimolecular reactions in the solution phase, where translational motions are constrained by the solvent.⁷ For example, binding of H₂ to catalyst **1** has an entropic cost ($T\Delta S$) of 8.3 kcal/mol at 1 atm. At a standard state of 1.0 mol/L, the entropic cost is lowered to 6.4 kcal/mol. At 9.625 mol/L (pure diethyl ether) the entropic cost is lowered to 5.1 kcal/mol. Another correction that has been proposed is to reduce $\Delta S_{\text{solution}}$ for bimolecular reactions to $2/3 \Delta S_{\text{gas}}$.⁸ This would be a very similar correction in our case.

¹ version 3.3 or later, <http://www.ccdc.cam.ac.uk/pages/Home.aspx>

² Gaussian 09, Revision D.01, M. J. Frisch, G. W. Trucks, H. B. Schlegel, G. E. Scuseria, M. A. Robb, J. R. Cheeseman, G. Scalmani, V. Barone, B. Mennucci, G. A. Petersson, H. Nakatsuji, M. Caricato, X. Li, H. P. Hratchian, A. F. Izmaylov, J. Bloino, G. Zheng, J. L. Sonnenberg, M. Hada, M. Ehara, K. Toyota, R. Fukuda, J. Hasegawa, M. Ishida, T. Nakajima, Y. Honda, O. Kitao, H. Nakai, T. Vreven, J. A. Montgomery, Jr., J. E. Peralta, F. Ogliaro, M. Bearpark, J. J. Heyd, E. Brothers, K. N. Kudin, V. N. Staroverov, T. Keith, R. Kobayashi, J. Normand, K. Raghavachari, A. Rendell, J. C. Burant, S. S. Iyengar, J. Tomasi, M. Cossi, N. Rega, J. M. Millam, M. Klene, J. E. Knox, J. B. Cross, V. Bakken, C. Adamo, J. Jaramillo, R. Gomperts, R. E. Stratmann, O. Yazyev, A. J. Austin, R. Cammi, C. Pomelli, J. W. Ochterski, R. L. Martin, K. Morokuma, V. G. Zakrzewski, G. A. Voth, P. Salvador, J. J. Dannenberg, S. Dapprich, A. D. Daniels, O. Farkas, J. B. Foresman, J. V. Ortiz, J. Cioslowski, and D. J. Fox, Gaussian, Inc., Wallingford CT, **2010**.

³ Legault, C. Y. CYLView, 1.0b; Université de Sherbrooke, Canada, **2009**; <http://www.cylview.org>.

⁴ (a) Grimme, S. *J. Comp. Chem.* **2006**, *27*, 1787. (b) Grimme, S.; Ehrlich, S.; Goerigk, L. *J. Comp. Chem.* **2011**, *32*, 1456.

⁵ (a) Weigend, F.; Ahlrichs, R. *Phys. Chem. Chem. Phys.* **2005**, *7*, 3297. (b) Weigend, F. *Phys. Chem. Chem. Phys.* **2006**, *8*, 1057.

⁶ Rohmann, K.; Holscher, M.; Leitner, W. *J. Am. Chem. Soc.* **2016**, *138*, 433.

⁷ (a) Martin, R. L.; Hay, P. J.; Pratt, L. R. *J. Phys. Chem. A* **1998**, *102*, 3565. (b) Sieffert, N.; Bühl, M. *Inorg. Chem.* **2009**, *48*, 4622.

⁸ Tobisch, S.; Ziegler, T. *J. Am. Chem. Soc.* **2004**, *126*, 9059.

For full cyclohexylphosphine ligand structures (**12-Cy**, **TS18-Cy**, **TS20-Cy**, and **TS22-Cy**), the size of the system (115 atoms) made optimization using a triple-zeta basis set impractical. Therefore, geometries were optimized and thermal corrections calculated using the smaller def2-SVP basis set. Single-point energy calculations were then performed on these structures using the larger def2-TZVP basis set. Conformational searches of the cyclohexyl groups were performed manually, considering up to 3 rotations for each Cy group. However, in the presence of the norbornene (or norbornyl) ligand, many of the possible rotamers were deemed impossible and a total of 9 conformations were examined for each structure. The lowest-energy conformation is consistent for each structure.

Intrinsic Reaction Coordinates

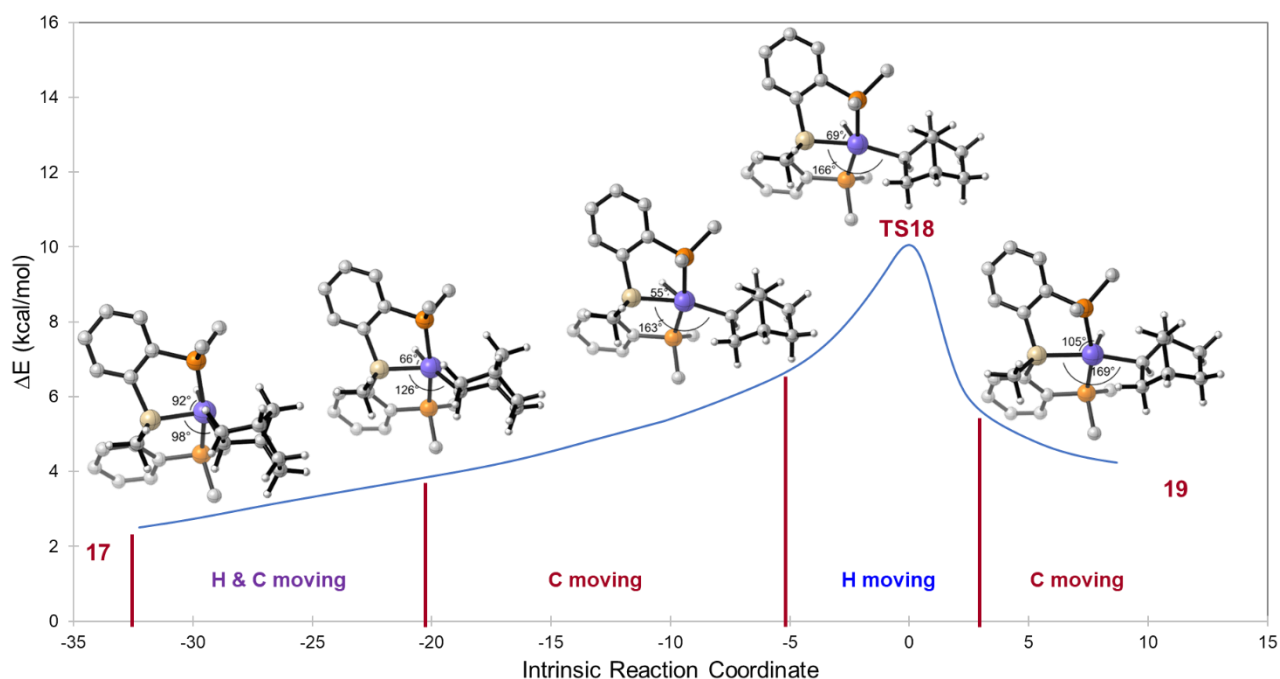


Figure S1. IRC analysis of **TS18** (norbornyl isomerization from **17** to **19**). Initially, the hydride moves in conjunction with the norbornyl ligand, maintaining an approximately 180° H-Rh-C angle. The H-Rh-Si angle decreases to about 60°, at which point the hydride stops and the reaction is dominated by norbornyl movement, resulting in a Y-shaped structure (IRC = -5). The hydride then moves back away from Si and the transition state is dominated by hydride motion from IRC = -5 to +5. The norbornyl then finishes moving trans to Si, giving **19**.

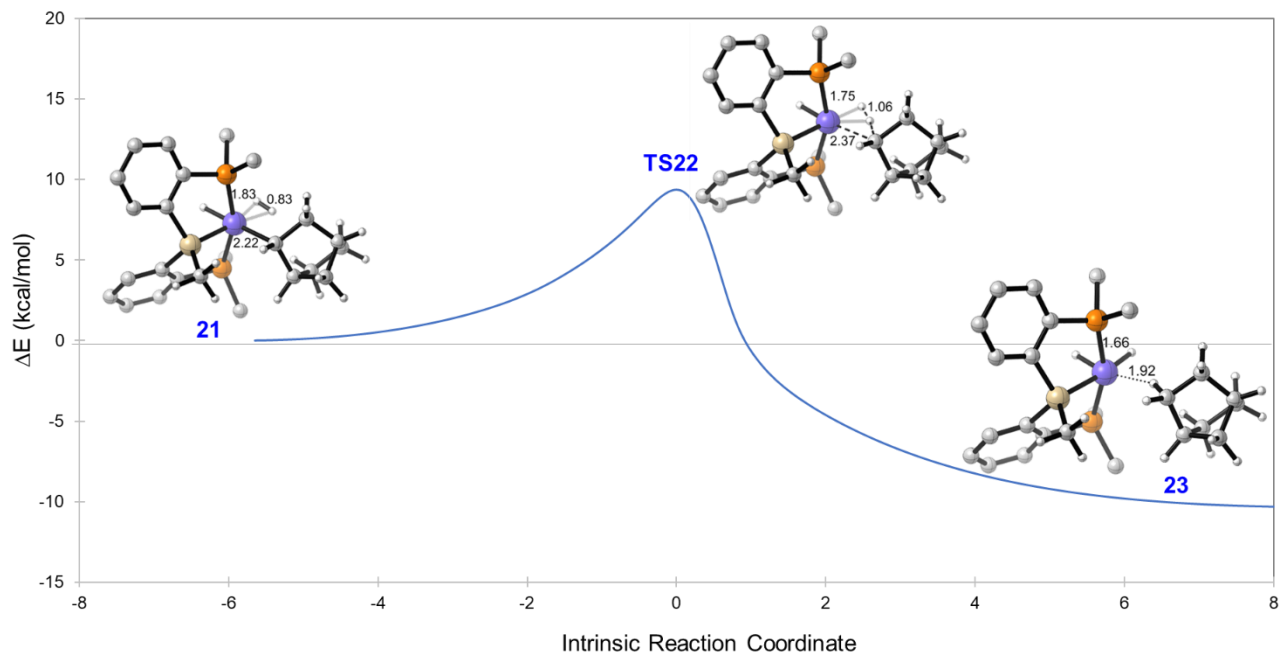


Figure S2. IRC analysis of TS22 (sigma-bond metathesis)

Additional Computed Structures

We considered both exo and endo hydrogenation of norbornene. As expected, reaction on the exo face is favored. For example, hydrometallation transition state **TS16-endo** is more than 10 kcal/mol higher in energy than exo **TS16** (Figure S3). Other points along the endo pathway are similarly disfavored.

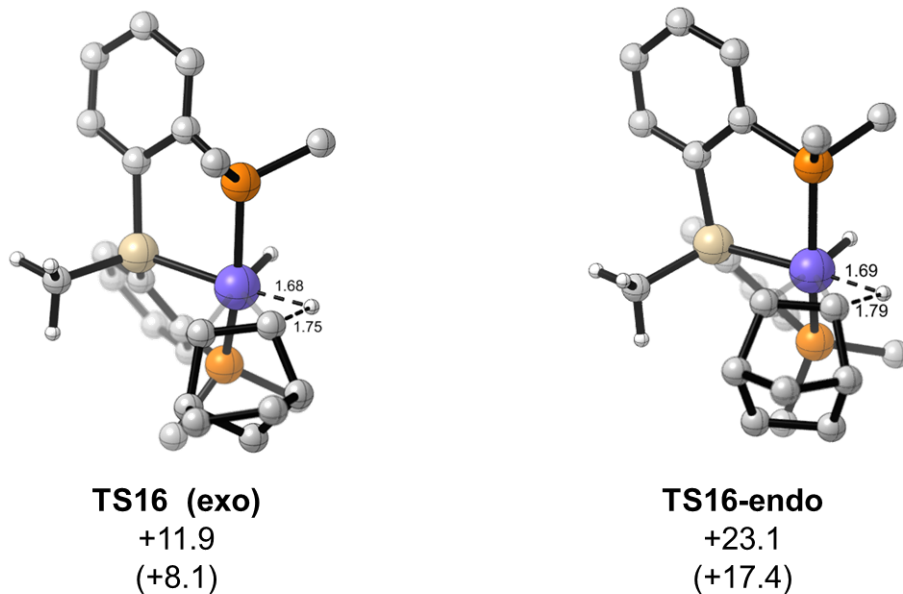


Figure S3. Exo and endo hydrometallation transition states **TS16** and **TS16-endo**. Gibbs free energies and enthalpies (in parentheses) in kcal/mol, with respect to the alkene complex **12** (exo).

The H₂-scrambling mechanism discussed in Figure 3 (main manuscript) has additional isomers possible (Figure S4). Complex **11** can undergo a second sigma-bond metathesis step (**SI-TS1**) to give dihydride **SI-2**, in which the H₂ molecule is anti to the Si-CH₃ bond. We find that sigma and pi complexes with this configuration are consistently disfavored.

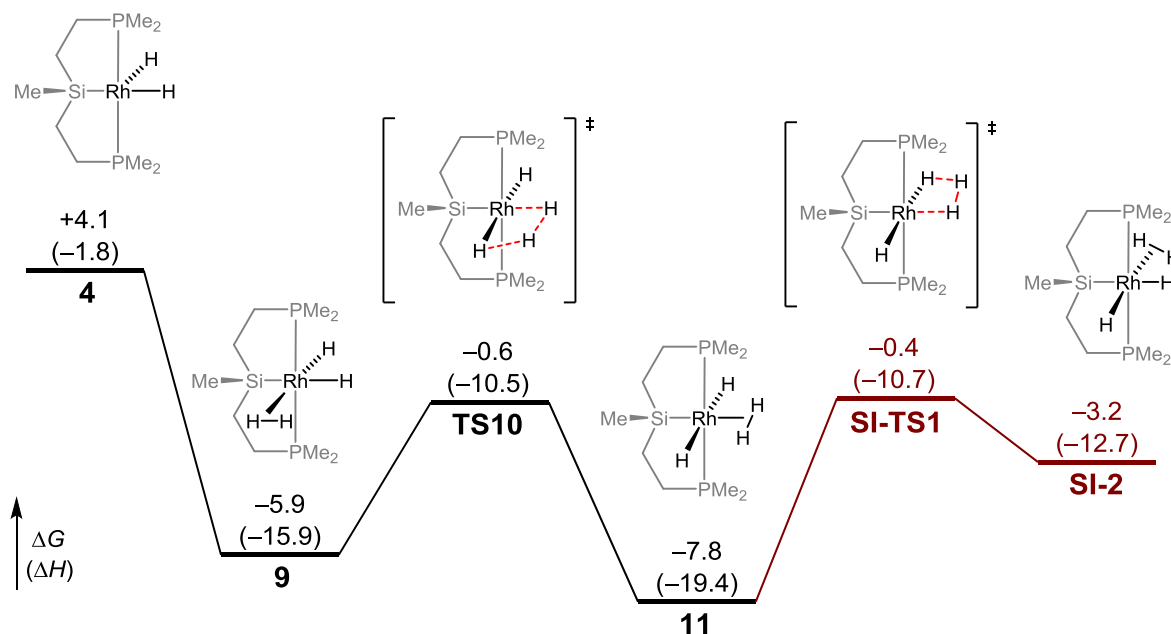


Figure S4. Full reaction pathway of model catalyst **1** with H₂ in the absence of alkene. Gibbs free energies and enthalpies (in parentheses) in kcal/mol.

We also considered an isomer of nba-complex **21** in which H₂ is trans to norbornyl (Figure S5). Formation of this isomer involves H-H-H sigma-bond metathesis (**SI-TS3**) instead of C-H-H sigma-bond metathesis. However, **SI-TS3** is about 4 kcal/mol higher in energy than either productive transition states (**TS18** or **TS22**), so this isomer is not likely and would not be expected to contribute to H-D scrambling.

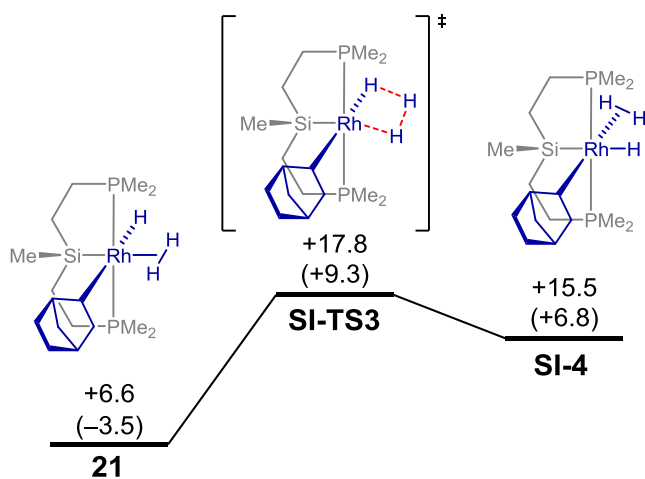


Figure S5. H₂-scrambling via sigma-bond metathesis of norbornyl complex **21**, which is disfavored compared to product formation (**TS22**, 14.0 kcal/mol). Gibbs free energies and enthalpies (in parentheses) in kcal/mol, with respect to the alkene complex **12**.

We located H₂-binding transition states (Figure S6) leading to σ -complex **13** (**SI-TS5**) and σ -complex **21** (**SI-TS6**). These transition states are nearly identical in energy to the respective σ -complex, so they do not have any impact on the free-energy profile.

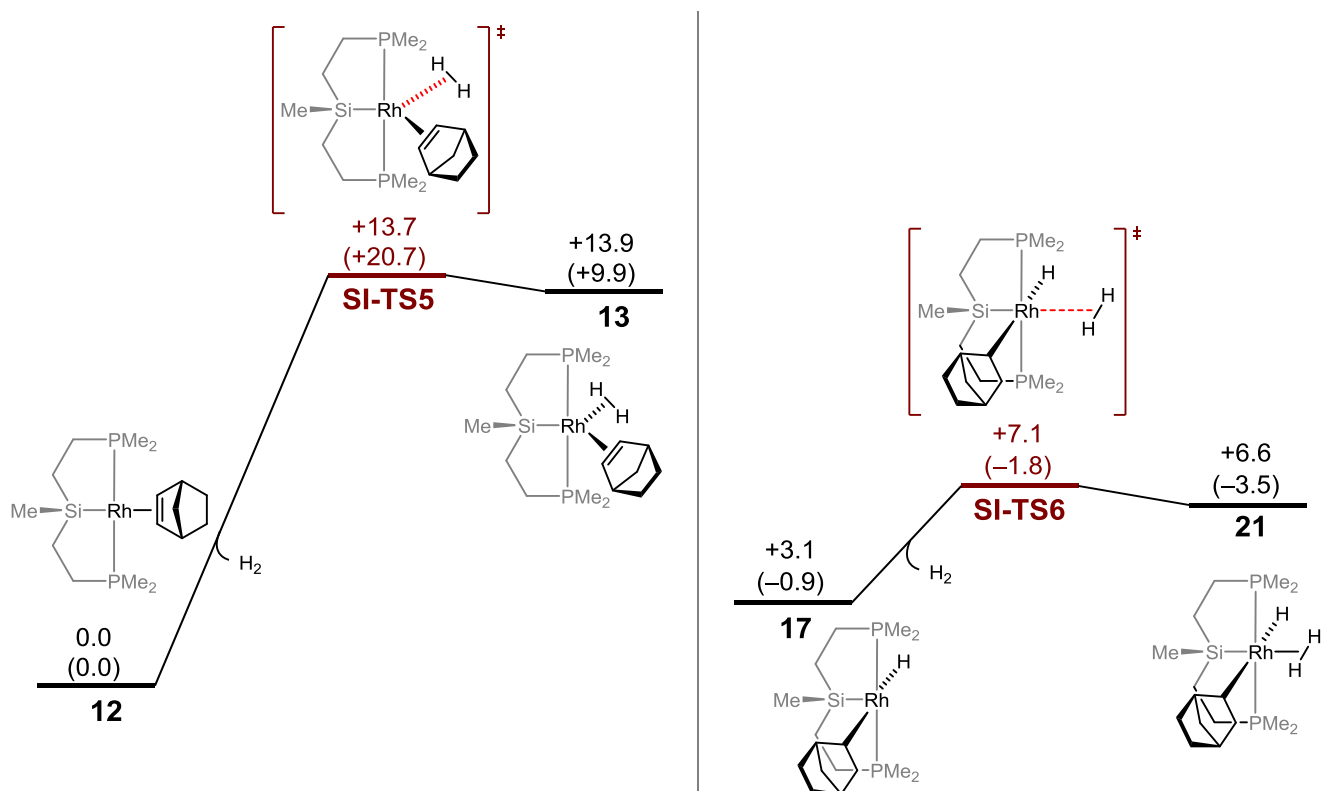


Figure S6. H₂-binding transition states leading to σ -complexes **13** and **21**. Gibbs free energies and enthalpies (in parentheses) in kcal/mol, with respect to the alkene complex **12**.

Tables of Computational Data

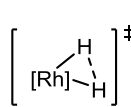
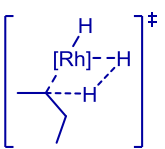
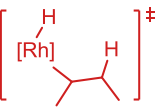
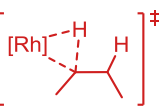
Table S1: SCF Energies and thermal corrections for all structures

Structure	SCF Energy (hartree)	H correct. (hartree)	G correct. (hartree)	H (hartree)	G (hartree)	ΔH (kcal/mol)	ΔG (kcal/mol)
1	-1744.706447	0.369901	0.297542	-1744.336546	-1744.408905	0.0	0.0
nbe	-272.6434597	0.155675	0.125930	-272.4877847	-272.5175293		
H2	-1.183622706	0.013240	0.003586	-1.170382706	-1.180036374		
nba	-273.8840415	0.179963	0.144933	-273.7040785	-273.7391085		
H2 Activation							
2	-1745.906944	0.385988	0.312030	-1745.520956	-1745.594914	-8.8	-3.7
TS3	-1745.892037	0.383648	0.311247	-1745.508389	-1745.580790	-0.9	5.1
4	-1745.895057	0.385206	0.312624	-1745.509851	-1745.582432	-1.8	4.1
TS5	-1745.894035	0.383655	0.311289	-1745.51038	-1745.582745	-2.2	3.9
6	-1745.909113	0.384517	0.311535	-1745.524596	-1745.597577	-11.1	-5.4
TS7	-1745.907778	0.383923	0.312956	-1745.523855	-1745.594822	-10.6	-3.7
8	-1745.909181	0.386556	0.311408	-1745.522625	-1745.597773	-9.8	-5.5
H2 Scrambling							
9	-1747.105751	0.403174	0.327295	-1746.702577	-1746.778456	-15.9	-5.9
TS10	-1747.093174	0.399168	0.323248	-1746.694006	-1746.769926	-10.5	-0.6
11	-1747.109509	0.401269	0.328142	-1746.70824	-1746.781366	-19.4	-7.8
SI-TS1	-1747.094305	0.400017	0.324666	-1746.694288	-1746.769639	-10.7	-0.4
SI-2	-1747.100242	0.402671	0.326198	-1746.697571	-1746.774044	-12.7	-3.2
SI-TS3	-2019.753622	0.56175	0.472898	-2019.191872	-2019.280724	-16.8	3.6
SI-4	-2019.761467	0.565675	0.477099	-2019.195792	-2019.284368	-19.3	1.3
NBE-bound H2 Activation							
12	-2017.392637	0.526775	0.443616	-2016.865862	-2016.949021	-26.1	-14.2
SI-TS5	-2018.560495	0.541245	0.453195	-2018.019250	-2018.107300	-15.4	-0.5
13	-2018.563879	0.543427	0.456905	-2018.020452	-2018.106974	-16.2	-0.3
TS14	-2018.562142	0.542843	0.453351	-2018.019299	-2018.108790	-15.4	-1.5
15	-2018.573391	0.54562	0.459519	-2018.027771	-2018.113872	-20.7	-4.6
TS16	-2018.566926	0.543602	0.456754	-2018.023324	-2018.110172	-18.0	-2.3
17	-2018.584727	0.547022	0.460580	-2018.037705	-2018.124147	-27.0	-11.1
TS16-endo	-2018.551264	0.542727	0.459021	-2018.008537	-2018.092243	-8.7	8.9
Reductive Elimination							
TS18	-2018.567824	0.546341	0.460088	-2018.021483	-2018.107736	-16.8	-0.8
19	-2018.578263	0.545402	0.462105	-2018.032861	-2018.116157	-23.9	-6.1
TS20	-2018.571438	0.546197	0.459602	-2018.025241	-2018.111836	-19.2	-3.4
24	-2018.606218	0.550343	0.462393	-2018.055875	-2018.143825	-38.4	-23.4

Structure	SCF Energy (hartree)	H correct. (hartree)	G correct. (hartree)	H (hartree)	G (hartree)	ΔH (kcal/mol)	ΔG (kcal/mol)
Sigma Bond Metathesis							
SI-TS6	-2019.770768	0.561272	0.467860	-2019.209496	-2019.297761	-27.9	-7.1
21	-2019.776330	0.564083	0.477735	-2019.212247	-2019.298595	-29.6	-7.6
TS22	-2019.760778	0.561743	0.474066	-2019.199035	-2019.286711	-21.3	-0.1
23	-2019.797334	0.566401	0.479830	-2019.230933	-2019.317504	-41.3	-19.5
Full Cy Ligand¹							
nbe	-272.6427795	0.155699	0.125963	-272.4870805	-272.5168162		
H2	-1.183465285	0.013150	0.003458	-1.170315285	-1.180006952		
1-Cy	-2525.932873	0.872115	0.755900	-2525.060758	-2525.176973	0.0	0.0
12-Cy	-2798.616381	1.030475	0.909662	-2797.585906	-2797.706718	-19.9	-6.7
TS18-Cy	-2799.794266	1.049632	0.925494	-2798.744634	-2798.868771	-12.6	4.6
TS20-Cy	-2799.795493	1.048270	0.922154	-2798.747223	-2798.873338	-14.2	1.8
TS22-Cy	-2800.987505	1.065629	0.939724	-2799.921876	-2800.047780	-16.9	5.3

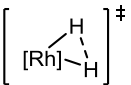
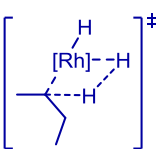
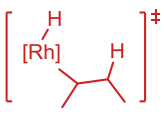
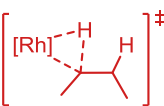
¹ Full Cy ligand structures and thermal corrections were calculated using B97-D3BJ/def2-SVP/IEF-PCM. Electronic energies were then calculated with the larger def2-TZVP basis set.

Table S2: Energies of key structures using different standard-state concentrations

Pressure / Concent.	H ₂ Activation			Bimolecular	Unimolecular		$\Delta\Delta G$ TS22 – TS22
							
35 atm (9.6 mol/L) pure Et ₂ O	-3.7	+5.1	+4.1	-0.1	-0.8	-3.4	+0.7
24 atm (1.0 mol/L)	-2.4	+6.5	+5.4	+3.9	+1.9	-0.7	+2.0
1 atm	-0.5	+8.3	+7.3	+9.6	+5.7	+3.1	+3.9

All values are ΔG with respect to catalyst **1**, and calculated using B97-D3BJ/def2-TZVP/IEF-PCM(diethyl ether). $\Delta\Delta G$ is the difference between rate-limiting steps in the bimolecular and unimolecular pathways. The unimolecular pathway (red) is favored, but by a much smaller amount at higher concentrations to account for decreased entropy in solution.

Table S3: Energies of key structures with different methods

Method	H ₂ Activation			Bimolecular	Unimolecular		$\Delta\Delta G$ TS22 – TS20
	 2	 TS3	 4	 TS22	 TS18	 TS20	
B97-D3, PCM	-3.7	+5.1	+4.1	-0.1	-0.8	-3.4	+0.7
B97-D, PCM	+0.2	+8.1	+7.6	+2.4	-0.2	-1.7	+2.6
B97-D, SMD	+0.1	+7.7	+6.0	+4.0	+0.6	-0.9	+3.4
B3LYP-D3, PCM	-4.4	+4.3	+3.1	+5.3	-1.1	-1.4	+2.4
B3LYP-D3, SMD	-3.3	+4.8	+1.6	+3.4	+0.1	+0.5	+2.8
M06L, PCM	-6.0	+5.5	+4.3	+0.7	-2.1	-4.1	+2.8
M11L, PCM	-3.5	+4.2	+3.1	+0.3	-2.2	-3.1	+2.5

All values are ΔG with respect to catalyst **1**, and calculated using the def2-TZVP basis set using an elevated pressure (235 atm) to account for entropy effects in solution. The rate-determining step of the favored pathway is indicated in bold. $\Delta\Delta G$ is the difference between rate-limiting steps in the bimolecular and unimolecular pathways. The unimolecular pathway (red) is favored by about 1–3 kcal/mol.

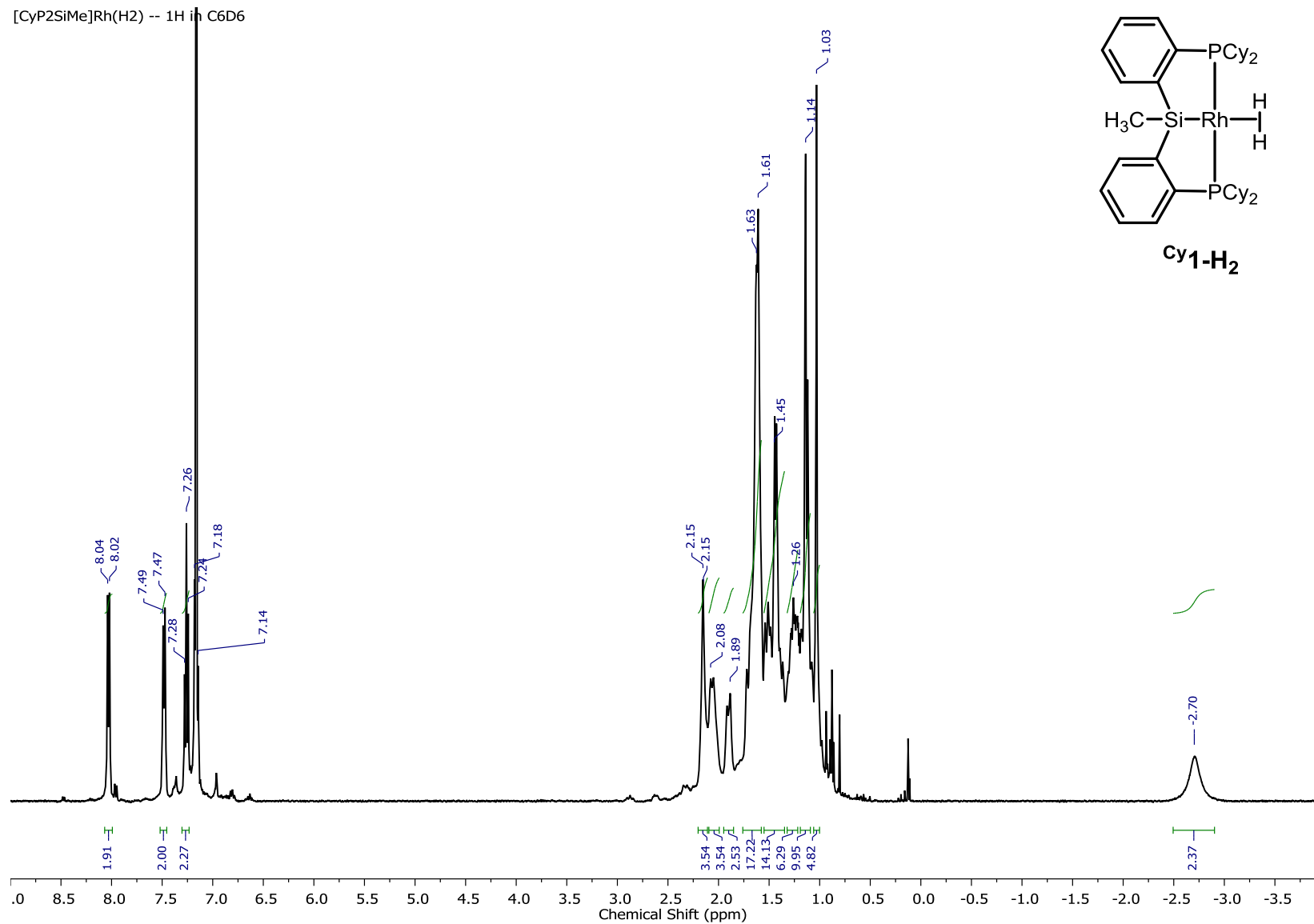


Figure S7. ¹H NMR spectrum of [^{Cy}P₂Si^{Me}]Rh(H)₂ (**Cy1-H₂**) in C₆D₆ measured on a 400 MHz Bruker Avance III

[CyP₂SiMe]Rh(H₂) -- 31P in C₆D₆

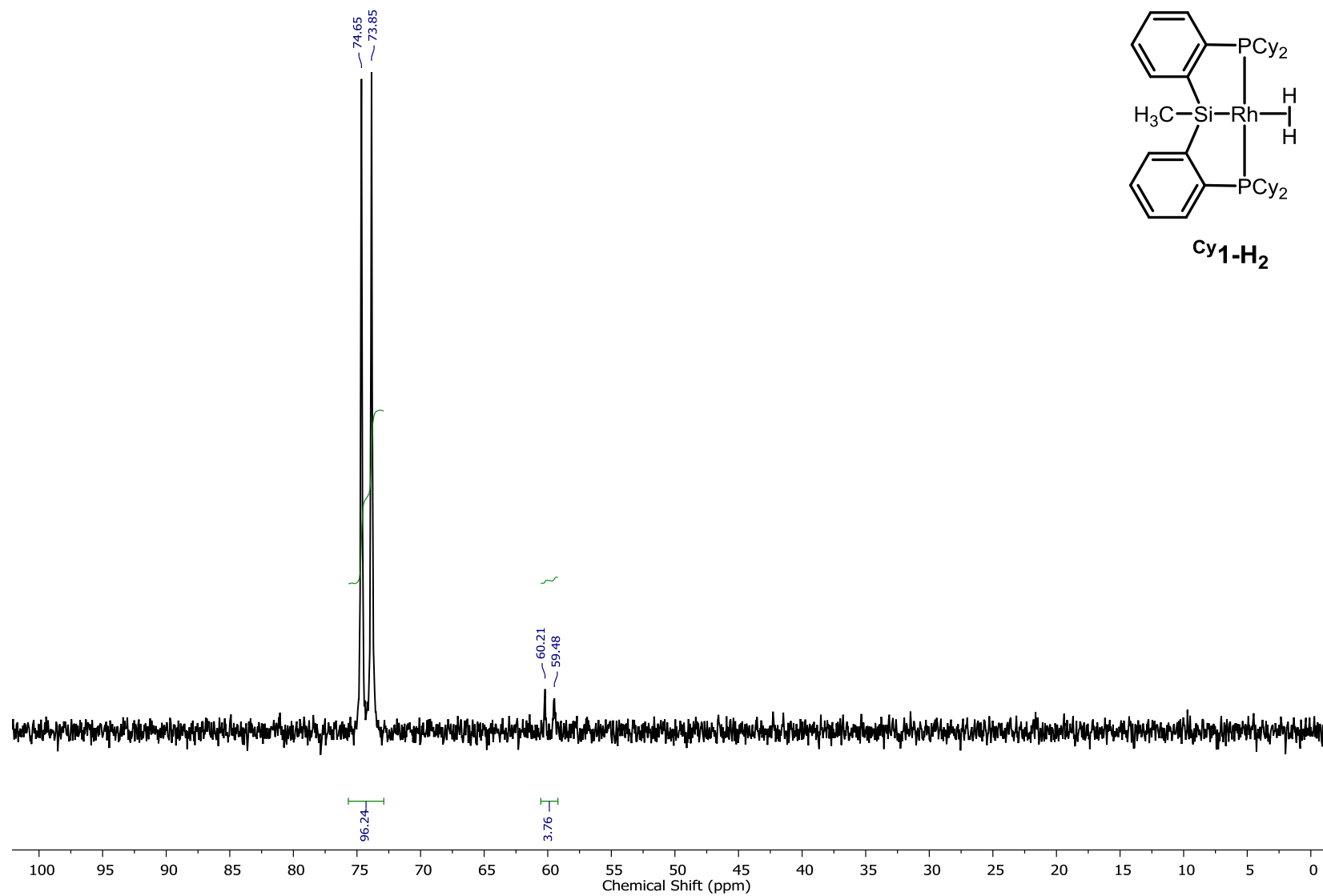


Figure S8. ³¹P NMR spectrum of [CyP₂Si^{Me}]Rh(H₂) (Cy1-H₂) in C₆D₆ measured on a 400 MHz Bruker Avance III

[CyP2SiMe]Rh(nbd) + HD - 1H in C6D6

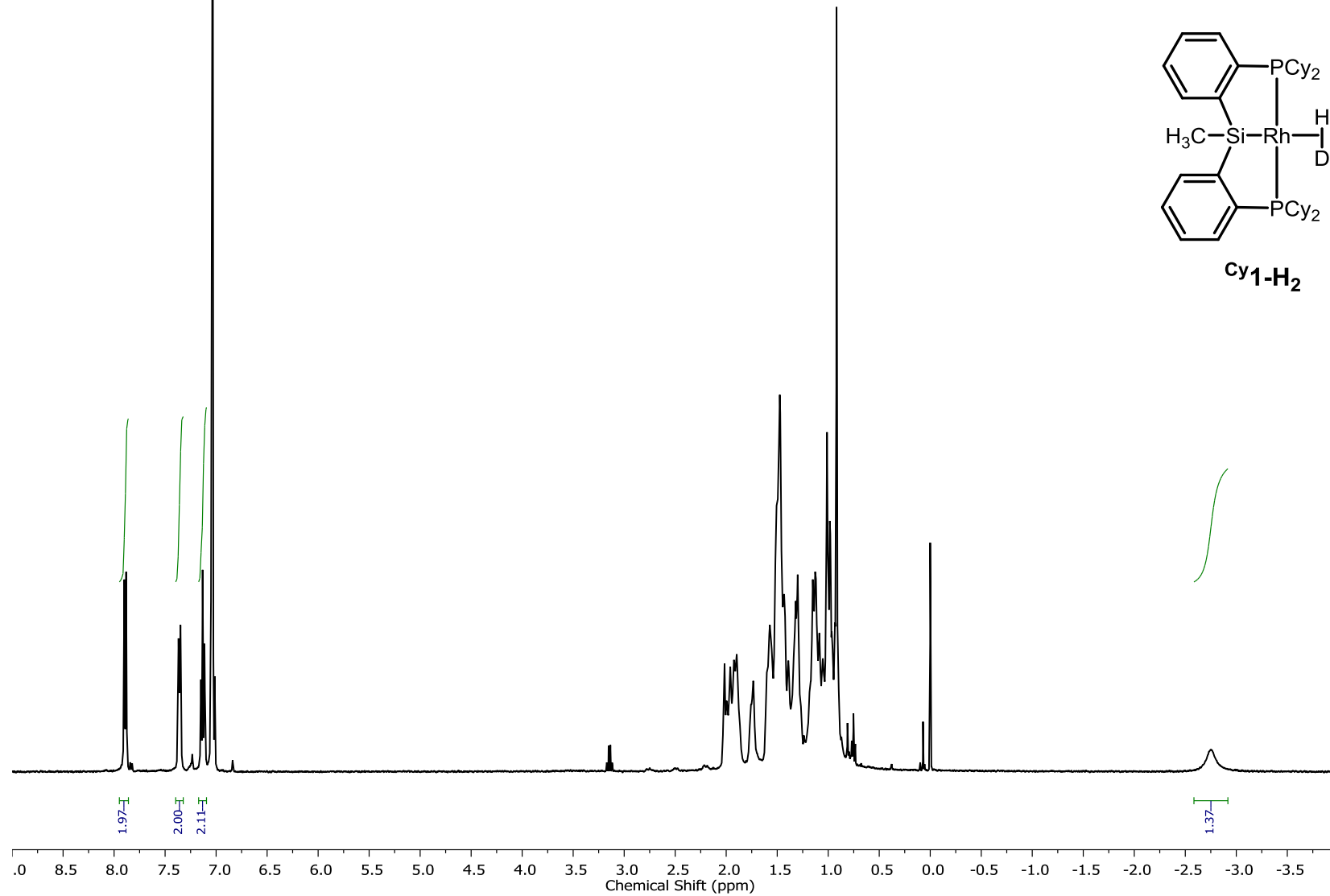
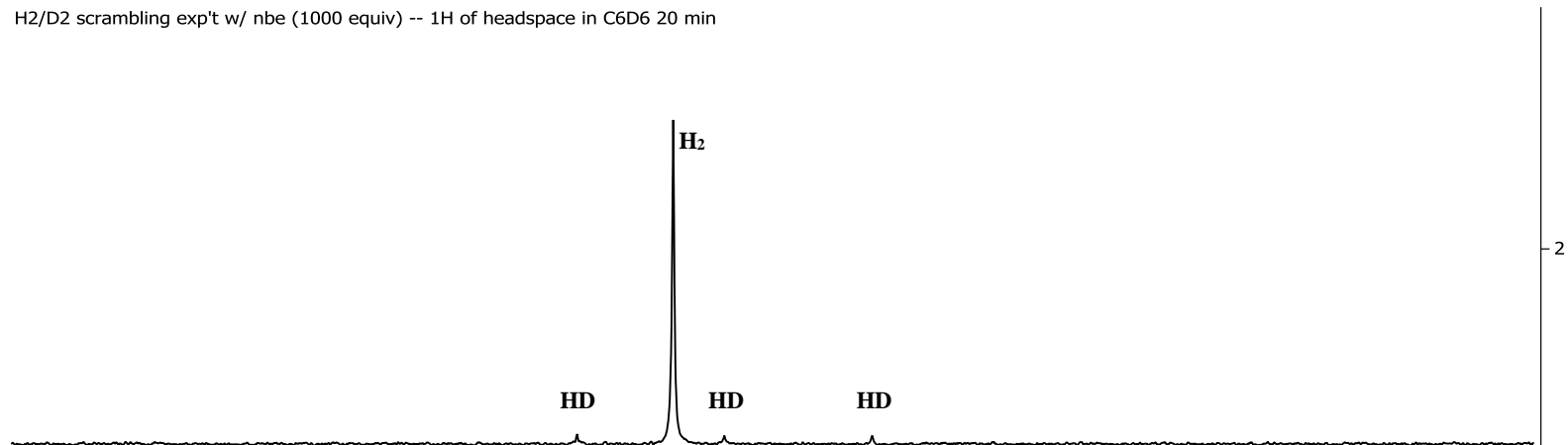
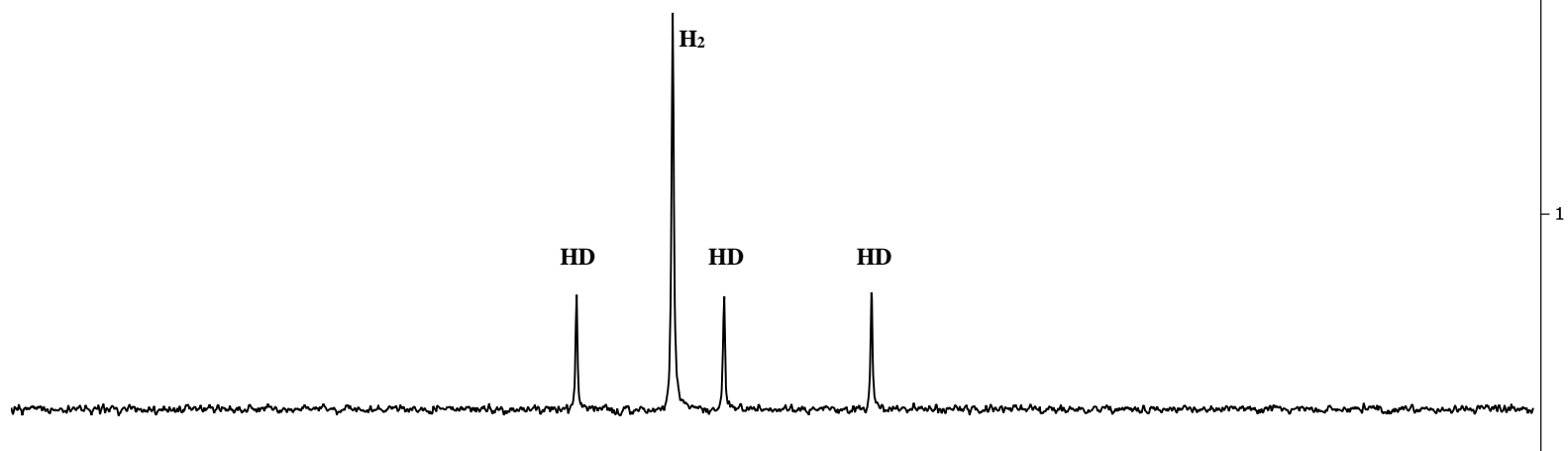


Figure S9. ¹H NMR spectrum of reaction product of [CyP₂Si^{Me}]Rh(nbd) (**Cy1-nbd**) with HD in C₆D₆ measured on a 400 MHz Bruker Avance III

H₂/D₂ scrambling exp't w/ nbe (1000 equiv) -- 1H of headspace in C₆D₆ 20 min



H₂/D₂ scrambling exp't w/o nbe present -- 1H of headspace in C₆D₆ 20 min



95 4.90 4.85 4.80 4.75 4.70 4.65 4.60 4.55 4.50 4.45 4.40 4.35 4.30 4.25 4.20 4.15 4.10 4.05 4.00 3.95 3.90 3.85
Chemical Shift (ppm)

Figure S10. ¹H NMR spectra of headspace after reaction of ^{Cy}**1-nbd** under 1:1 H₂/D₂ (1 atm) for 20 min in the presence (top) and absence (bottom) of excess (1000 equiv) norbornene

Determination of Norbornane Isotopomer Distribution in HD Reactions

Hydrogenation of norbornene (nbe) under HD can produce 3 possible isotopomers: nba- d_0 , - d_1 , and - d_2 . The percentage of each isotopomer in the resulting mixture can be determined by modeling the relative peak intensities in electron-impact mass spectra corresponding to the m/z 96.1, 97.1, and 98.1 (molecular ion peaks for the d_0 , d_1 , and d_2 isotopomers, respectively). Shown below is an excerpt of the mass spectrum for pure nba- d_0 .

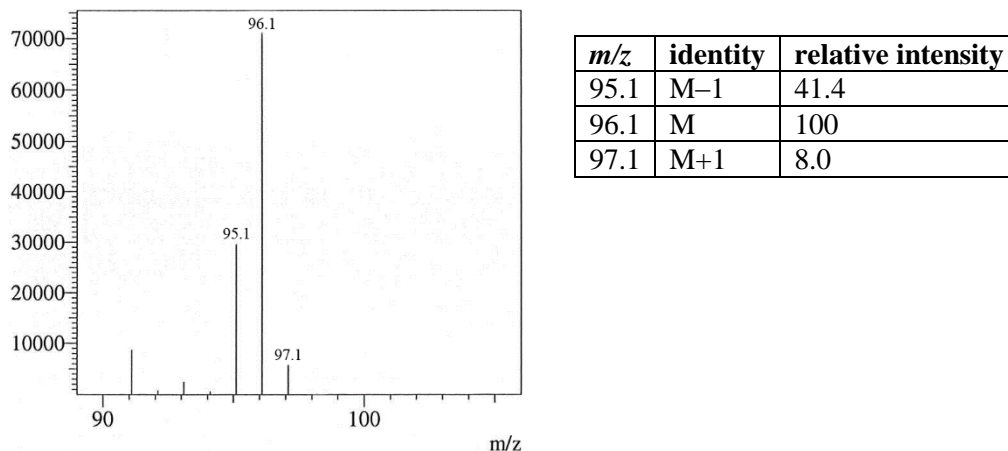


Figure S11. Mass spectrum of norbornane

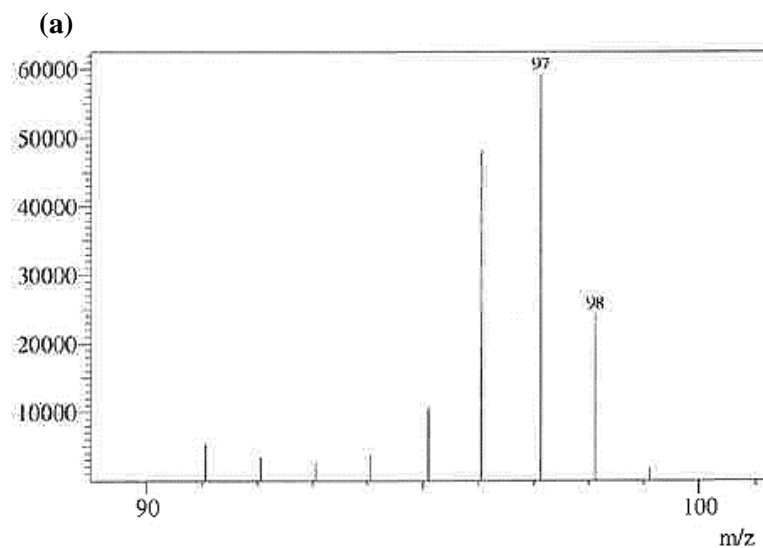
In a mass spectrum containing nba- d_0 , - d_1 , and - d_2 , the m/z 95.1, 96.1, 97.1, and 98.1 peaks represent the following combinations:

$$\begin{aligned}
 m/z\ 95.1: & [M-1]_{d0} \\
 m/z\ 96.1: & [M]_{d0} + [M-1]_{d1} \\
 m/z\ 97.1: & [M+1]_{d0} + [M]_{d1} + [M-1]_{d2} \\
 m/z\ 98.1: & [M+1]_{d1} + [M]_{d2}
 \end{aligned}$$

Thus, the following system of equations can be constructed, where χ_{dn} represents the mole fraction of the dn isotopomer ($n = 0, 1, \text{ or } 2$) in the norbornane mixture:

$$\begin{aligned}
 I_{95.1} &= 41.4\chi_{d0} \\
 I_{96.1} &= 100\chi_{d0} + 41.4\chi_{d1} \\
 I_{97.1} &= 8.0\chi_{d0} + 100\chi_{d1} + 41.1\chi_{d2} \\
 I_{98.1} &= 8.0\chi_{d1} + 100\chi_{d2}
 \end{aligned}$$

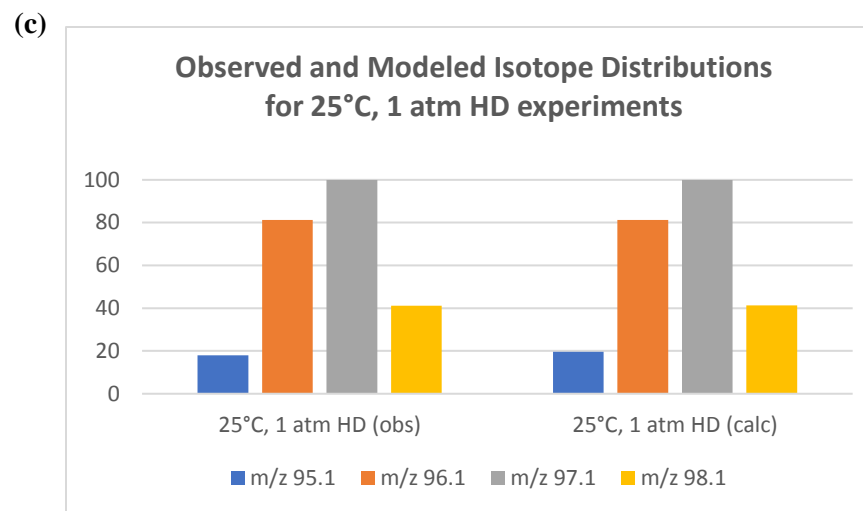
The peak distributions were fit empirically to the m/z 96.1, 97.1, and 98.1 peaks, and calculated isotope patterns shown in Figures S5–S7 also include the m/z 95.1 peak, which was not fit but matches the observed data reasonably well.



(b)

Distribution of norbornane isotopomers

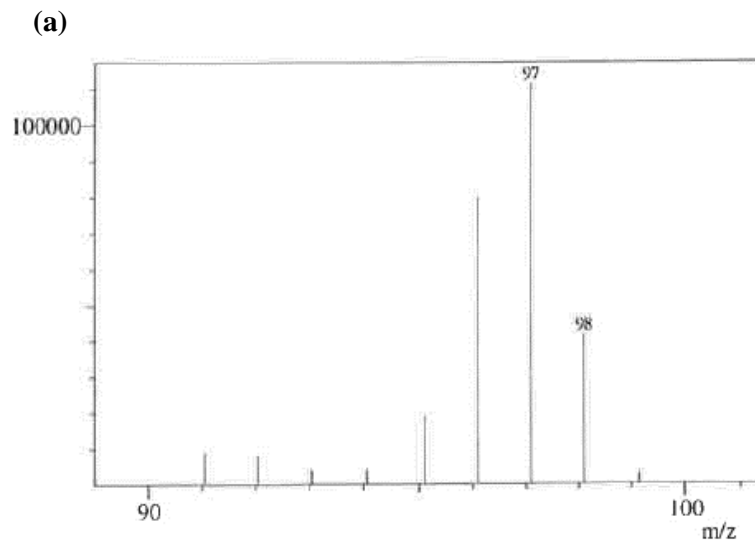
nba- d_0	28.9%
nba- d_1	49.9%
nba- d_2	21.2%



(d)

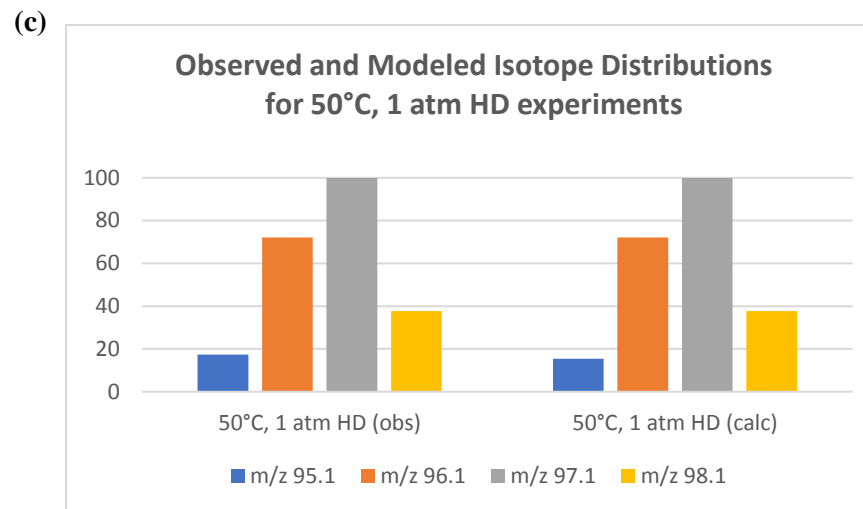
m/z	relative intensity	
	observed	calculated
95.1	18.0	19.6
96.1	81.2	81.2
97.1	100	100
98.1	41.2	41.2

Figure S12. Hydrogenation of norbornene under HD (1 atm, 25 °C): (a) Partial mass spectrum of mixture of norbornane isotopomers. (b) Distribution of norbornane isotopomers based on modeling the relative intensities of m/z 96.1, 97.1, and 98.1 peaks. (c) Observed and calculated isotope distributions for m/z 95.1, 96.1, 97.1, and 98.1 peaks. (d) Numerical data corresponding to graph in (c).



(b)

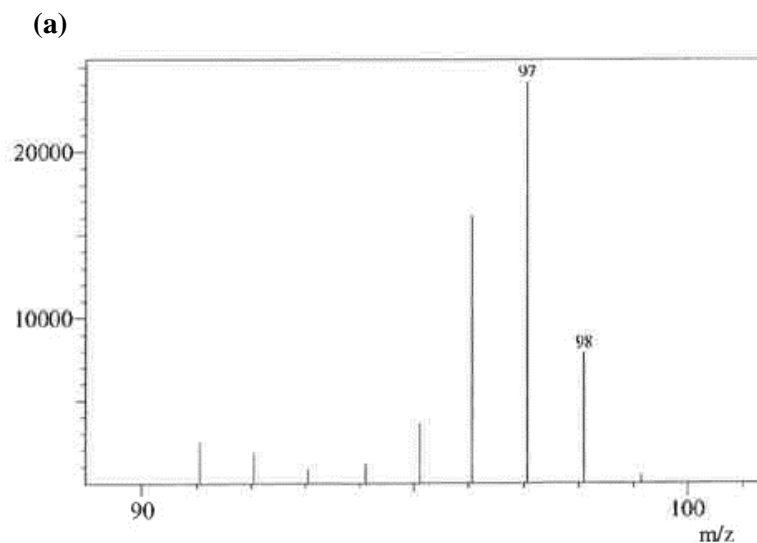
Distribution of norbornane isotopomers	
nba- d_0	24.4%
nba- d_1	55.2%
nba- d_2	20.3%



(d)

m/z	relative intensity	
	observed	calculated
95.1	17.4	15.4
96.1	72.1	72.1
97.1	100	100
98.1	37.7	37.7

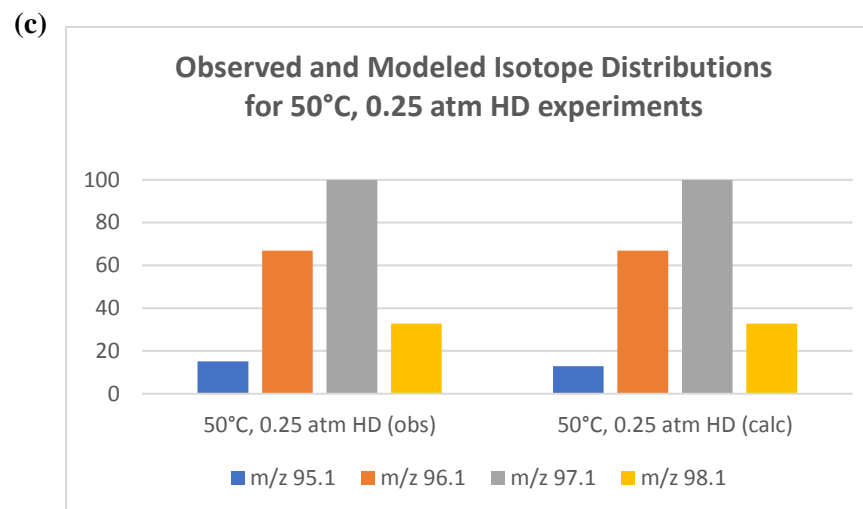
Figure S13. Hydrogenation of norbornene under HD (1 atm, 50 °C): (a) Partial mass spectrum of mixture of norbornane isotopomers. (b) Distribution of norbornane isotopomers based on modeling the relative intensities of m/z 96.1, 97.1, and 98.1 peaks. (c) Observed and calculated isotope distributions for m/z 95.1, 96.1, 97.1, and 98.1 peaks. (d) Numerical data corresponding to graph in (c).



(b)

Distribution of norbornane isotopomers

nba- d_0	21.5%
nba- d_1	60.5%
nba- d_2	18.0%



(d)

m/z	relative intensity	
	observed	calculated
95.1	15.1	12.8
96.1	66.9	66.9
97.1	100	100
98.1	32.8	32.8

Figure S14. Hydrogenation of norbornene under HD (0.25 atm, 50 °C): (a) Partial mass spectrum of mixture of norbornane isotopomers. (b) Distribution of norbornane isotopomers based on modeling the relative intensities of m/z 96.1, 97.1, and 98.1 peaks. (c) Observed and calculated isotope distributions for m/z 95.1, 96.1, 97.1, and 98.1 peaks. (d) Numerical data corresponding to graph in (c).